

Diagnosis of inter-turn short circuit fault in IPMSMs based on the combined use of greedy tracking and random forest

Jianping WANG, Jian MA[✉], Dean MENG*, Xuan ZHAO, Kai ZHANG, Qiquan LIU, and Kejie XU

School of Automobile, Chang'an University, Xi'an 710064, China

Abstract. Inter-turn short circuit (ITSC) is a frequent fault of interior permanent magnet synchronous motors (IPMSM). If ITSC faults are not promptly monitored, it may result in secondary faults or even cause extensive damage to the entire motor. To enhance the reliability of IPMSMs, this paper introduces a fault diagnosis method specifically designed for identifying ITSC faults in IPMSMs. The sparse coefficients of phase current and torque are solved by clustering shrinkage stage orthogonal matching tracking (CcStOMP) in the greedy tracking algorithm. The CcStOMP algorithm can extract multiple target atoms at one time, which greatly improves the iterative efficiency. The multiple features are utilized as input parameters for constructing the random forest classifier. The constructed random forest model is used to diagnose ITSC faults with the results showing that the random forest model has a diagnostic accuracy of 98.61% using all features, and the diagnostic accuracy of selecting three of the most important features is still as high as 97.91%. The random forest classification model has excellent robustness that maintains high classification accuracy despite the reduction of feature vectors, which is a great advantage compared to other classification algorithms. The combination of greedy tracing and the random forest is not only a fast diagnostic model but also a model with good generalisation and anti-interference capability. This non-invasive method is applicable to monitoring and detecting failures in industrial PMSMs.

Keywords: Inter-turn short circuit (ITSC); Interior permanent magnet synchronous motors (IPMSM); Matching-Pursuit (CcStOMP) algorithm; sparse coefficients; random forest.

1. INTRODUCTION

With the performance advantages of lightweight, dependable operation, low noise and high efficiency, permanent magnet synchronous motors (PMSMs) [1] have been widely used in industrial production. According to the arrangement of the permanent magnets, permanent magnet synchronous motors can be divided into surface-mounted permanent magnet synchronous motors (SPMSMs) and interior permanent magnet synchronous motors (IPMSMs). In comparison to SPMSMs, the rotor's embedded permanent magnet structure provides IPMSMs with greater torque density, enhanced structural robustness, and increased weak magnetic expansion capability. Owing to these advantages, vehicles with stringent traction performance requirements frequently opt for the utilization of IPMSMs as their traction motors.

Inter-turn short circuit (ITSC) fault is common in PMSMs and is mainly caused by insulation failure between adjacent windings in the coil [2]. When ITSC occurs, it leads to uneven magnetic field distribution, unbalanced three-phase current, and can cause the motor to burn up quickly. Once an ITSC fault occurs, it can lead to a significant drop in performance, costly operational losses and even fatal accidents. Therefore, the detection of a fault

in the first place can prevent it from progressing to a worse level and thus reduce industrial costs.

Upon the occurrence of an ITSC fault, various complex fault phenomena may manifest, often accompanied by alterations in characteristic signals. The basic idea is to extract the fault characteristics from the signal to identify the fault [3]. For ITSC fault detection, current [4–6], vibration [7–9], torque [10, 11] signals were mainly used. The use of a single signal analysis does not allow an in-depth analysis of fault characteristics, and many researchers made the fault diagnosis studies from a multi-signal perspective [12–15].

Sparse representation is an emerging linear representation theory that belongs to the data-driven category. Its goal is to represent the original data with as few elements as possible by representing the original signal with a sparse linear aggregate of over-complete dictionary atoms [16]. Consequently, it can effectively represent the fundamental features of the signal during the compression process. It can be used to denoise, resist interference and reduce the data space. Since it was proposed, sparse representations have been used in many technical fields [17]. The fault feature components can be extracted and reconstructed from the signal by sparse representation [15]. Owing to its outstanding interference immunity and efficient representation, it has emerged as a widely adopted research technique in the field of mechanical fault detection in recent years. Zhang *et al.* [18] constructed a weighted sparse model for bearing fault diagnosis. He *et al.* [19] applied sparsity to rotating machinery

*e-mail: deanmeng@chd.edu.cn

Manuscript submitted 2023-03-14, revised 2023-12-18, initially accepted for publication 2024-01-03, published in March 2024.

fault diagnosis. In these studies, sparse representation theory was mainly applied to the diagnosis of mechanical faults in motors, with less application to electrical faults. The characteristic signals are mostly based on vibration signals and almost rarely use electrical signals and moment signals.

The critical step in the sparse representation process is the solution to the sparse coefficients. To solve the sparse coefficients, greedy tracking algorithms were generally used. The Matching Pursuit (MP) algorithm was initially proposed in 1993. Due to the tautological selection of identical atoms during iterations, MP exhibits slow convergence in the iteration process. Donoho *et al.* [20] put forward the stage orthogonal matching tracking (StOMP) algorithm. StOMP can attain multi-atom extraction in each iteration by weakening the criteria for atom selection, thus greatly enhancing the convergence rate. The signal recovery effect is reduced due to the addition of many redundant atoms in the support set. Song *et al.* [21] proposed a clustering shrinkage stage orthogonal matching tracking (CcStOMP) algorithm that introduced the clustering shrinkage mechanism into atom selection. To enhance the matching rate, the support set was restricted by the clustering method. The accuracy of atomic matching was increased with the improvement of the convergence rate.

Machine learning has become a popular technique and has been widely used in the field of motor fault detection. Random forests (RF) algorithm has a strong advantage due to their stability and resistance to overfitting. However, the main application of the RF algorithm is induction motors fault detection. It is rarely applied to IPMSM fault classification.

A fault diagnosis method based on combined use of greedy tracking (CcStOMP) and RF is proposed for the existing ITSC fault diagnosis model of IPMSM with incomplete fault feature mining, low resolution characteristics and poor anti-interference capability. CcStOMP is used to solve the sparse coefficients of the current and torque signals, which are used to extract feature vectors which are fed into a RF classifier for training. Finally, the trained RF model is used for fault diagnosis. The detection algorithm is conducted offline, wherein the signals from the motor under test are collected through experiments. These signals are then processed using the corresponding algorithm model to obtain diagnostic results. The ITSC mathematical model is described in Section 2. In Section 3, the principles of CcStOMP and the random forest algorithm are described. The soundness of the algorithm was verified by experimentation in Section 4. The discussion of the results is provided in Section 5. Conclusions are given in Section 6.

2. MATHEMATICAL MODEL OF PMSM UNDER ITSC FAULT

To investigate the alterations in the relevant parameters of a PMSM during an ITSC fault, the equivalent schematic of a PMSM under such a circuit fault is designed, as illustrated in Fig. 1. It is assumed that the ITSC fault occurs on the A-phase stator winding of the PMSM. In the diagram, a short circuit is added to the A-phase winding of the motor. The short circuit resistor R_f divides the A-phase winding into two parts, $a1$ and $a2$, where $a1$ represents the normal part and $a2$ is the faulty

part. The current i_f is the short circuit current flowing through the resistor R_f . R_f represents the actual resistance of the short-circuit branch.

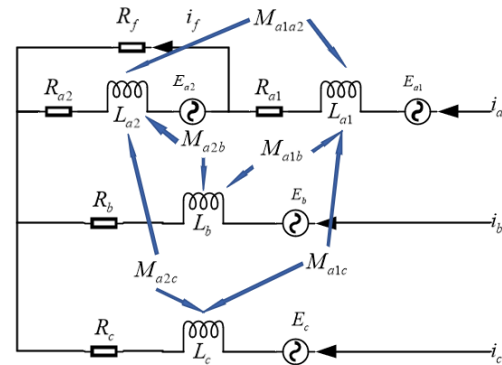


Fig. 1. Three-phase equivalent circuit model

The voltage equation [22] for a PMSM when ITSC fault occurs is

$$\mathbf{V}_{sf} = \mathbf{R}_{sf} \mathbf{i}_{sf} + \mathbf{L}_{sf} \frac{d\mathbf{i}_{sf}}{dt} + \mathbf{E}_{sf}, \quad (1)$$

where

$$\mathbf{V}_{sf} = [V_a \quad V_b \quad V_c \quad 0]^T,$$

$$\mathbf{u} = \frac{n}{N},$$

$$\mathbf{R}_{sf} = \begin{bmatrix} R_{a1}+R_{a2} & 0 & 0 & -R_{a2} \\ 0 & R_b & 0 & 0 \\ 0 & 0 & R_c & 0 \\ R_{a2} & 0 & 0 & -u(R_{a1}+R_{a2})-R_f \end{bmatrix},$$

$$\mathbf{i}_{sf} = [i_a \quad i_b \quad i_c \quad 0]^T,$$

$$\mathbf{L}_{sf} = \begin{bmatrix} L_{a1}+L_{a2}+2M_{a1a2} & M_{a1b}+M_{a2b} & M_{a1c}+M_{a2c} & -L_{a2}-M_{a1a2} \\ M_{a1b}+M_{a2b} & L_b & M_{bc} & -M_{a2b} \\ M_{a1c}+M_{a2c} & M_{bc} & L_c & -M_{a2c} \\ L_{a2}+M_{a1a2} & M_{a2b} & M_{a2c} & -L_{a2} \end{bmatrix},$$

$$\mathbf{E}_{sf} = \begin{bmatrix} E_a \\ E_b \\ E_c \\ E_f \end{bmatrix}$$

$$= \begin{bmatrix} \lambda_{PM,1} \cos(\theta) + \sum_{v=2k+1} \lambda_{PM,v} \cos(v\theta - \theta_v) \\ \lambda_{PM,1} \cos\left(\theta - \frac{2\pi}{3}\right) + \sum_{v=2k+1} \lambda_{PM,v} \cos\left(v\theta - \theta_v - v\frac{2\pi}{3}\right) \\ \lambda_{PM,1} \cos\left(\theta + \frac{2\pi}{3}\right) + \sum_{v=2k+1} \lambda_{PM,v} \cos\left(v\theta - \theta_v + v\frac{2\pi}{3}\right) \\ u \left(\lambda_{PM,1} \cos(\theta) + \sum_{v=2k+1} \lambda_{PM,v} \cos(v\theta - \theta_v) \right) \end{bmatrix},$$

where n is the number of short-circuit turns of the stator winding of a phase; N is the total number of turns of the stator winding of a phase; V_{sf} is the phase voltage matrix of the stator winding; R_{sf} is the resistance matrix; i_{sf} is the current matrix; L_{sf} is the inductance matrix; E_{sf} is the back electromotive force matrix; R_f is the fault resistance; R_{a1} , R_{a2} , R_b and R_c are the resistances; i_a , i_b and i_c are the currents in the stator windings; i_f is the short-circuit current; L_{a1} , L_{a2} , L_b and L_c are the self-inductances; M is the mutual inductance between the stator windings; $\lambda_{PM,1}$ is the fundamental amplitude of the magnet flux; $\lambda_{PM,v}$ is the v -th harmonic amplitude of the magnet flux; θ is the rotor electric angle; θ_v is the angle between the fundamental and v -th harmonic of the magnet flux.

By disregarding the higher harmonics of the permanent magnet's magnetic field, the electromagnetic torque of the PMSM with an ITSC fault can be calculated as

$$T_c = \frac{P_n}{2} i_{sf} \Lambda_{PM,1} \begin{bmatrix} \cos(\theta) \\ \cos(\theta - 2\pi/3) \\ \cos(\theta + 2\pi/3) \\ u \cos(\theta) \end{bmatrix}. \quad (2)$$

3. METHODOLOGY

3.1. Greedy tracking through CcStOMP

The theory of sparse representation is to convert a non-sparse original signal into sparse coefficients through a dictionary matrix. The sparse coefficients are used to represent the original signal. Sparse representation is also known as sparse coding [23].

For an input signal $\mathbf{y} = [y_0, y_1, \dots, y_n]^T$ of length n , the formula for the sparse representation is as follows:

$$\mathbf{y} = \mathbf{D}\mathbf{x}, \quad (3)$$

where $\mathbf{D} = [\mathbf{d}_0, \mathbf{d}_1, \dots, \mathbf{d}_m]$ is a dictionary matrix whose column vector $\mathbf{d}_i \in \mathbb{R}^{n \times 1}$ is called a dictionary atom and satisfies $\|\mathbf{d}_i\| = 1$. $\mathbf{x} = [x_0, x_1, \dots, x_m]^T$ is the solution to the sparse representation, i.e. the sparse representation coefficients. Expand the equation in matrix form:

$$\mathbf{y} = \sum_{i=1}^n \mathbf{x}_i \mathbf{d}_i. \quad (4)$$

When the size of the dictionary matrix is $m = n$, the matrix is square. This dictionary is called a complete dictionary. A complete dictionary may not meet the requirements of sparse representation. The dictionary required for sparse representation needs to satisfy $n < m$, in which the number of atoms is much larger than the signal length. This dictionary is called an overcomplete dictionary.

The discrete cosine transform (DCT) dictionary is commonly used in the construction of dictionaries for sparse expressions. DCT expresses the original signal by using the combination of several cosine functions with different oscillation frequencies. Like the Fourier transform, DCT is well-suited for decomposing

periodic signals, such as the current in PMSMs. Wang *et al.* [23] demonstrated that a good approximation of the original signal can be made by DCT without the need for many cosine basis functions. Meanwhile, in contrast to the Fourier transform, the approximation can be achieved with only half of the information and the computation is faster. The DCT dictionary has become a common dictionary on sparse representation and compressive sensing.

A common method used for solving problems with sparse coefficients is the greedy tracing algorithm. 'Greedy' implies a strategy of making a "hard" decision based on some local optimum at each iteration step. For a given \mathbf{x} , we wish to recover an approximately k sparse vector α such that the following assumptions hold: the error $e \in \mathbb{R}^m$ is bounded and the dictionary matrix \mathbf{D} satisfies the Restricted Isometry Property (RIP):

$$(1 - \delta_{2k}) \|\mathbf{x}\|_2^2 \leq \|\mathbf{D}\mathbf{x}\|_2^2 \leq (1 + \delta_{2k}) \|\mathbf{x}\|_2^2, \quad (5)$$

\mathbf{x} is an arbitrary $2k$ sparse vector with $0 \leq \delta_{2k} < 1$.

This type of method builds up an estimation of \mathbf{x} by Iteration. The algorithm takes the zero value as the initial value and gradually adds new elements that are determined to be non-zero. These non-zero values are estimated at each step of the iteration using an optimization approach. This method can handle larger data sets rapidly.

Greedy tracking involves the following two steps: atomic selection and coefficient update. These methods typically use a zero value as the initial estimate, $\hat{\mathbf{x}}^{[0]} = \mathbf{0}$. After initialisation, the initial residual can be expressed as $\mathbf{r}^{[0]} = \mathbf{y} - \mathbf{A}\hat{\mathbf{x}}^{[0]} = \mathbf{y}$. The set of support sets for the initial estimate is the empty set $\mathbf{T} = \emptyset$. It adds additional atoms (columns of the matrix \mathbf{A}) to the set of support sets \mathbf{T} and updates the estimation of the signal $\hat{\mathbf{x}}$ in each iteration, thereby reducing the observation error.

In CcStOMP, a cluster shrinkage technique is introduced to the atom matching step to filter out the selected atoms by the threshold criterion [21]. This approach enhances the rate of atom matching. The whole flow of CcStOMP is presented below.

CcStOMP Algorithm flow

Input: original signal $\tilde{\mathbf{y}} \in \mathbb{R}^n$, tailored dictionary \mathbf{D} , maximum distance maxdist

Initialization: residual $\mathbf{r}_0 = \mathbf{x}$, support set $\mathbf{T} = \emptyset$, maximum number of iterations ite

Loop: for $t = 1$ to ite do

1. Calculate $\langle r_{t-1} \alpha_i \rangle, 1 \leq i \leq K$;
 2. Select atoms $J_t = \{\alpha_j \mid \langle r_{t-1}, \alpha_j \rangle \geq Th_{t-1}\}$
 3. Cluster-contraction method, obtain F_t from J_t
 4. Extend support set $T_t = T_{t-1} \cup F_t$
 5. Determine the weights $\theta_t = T_t^* \tilde{\mathbf{y}}$
 6. Update residuals $\mathbf{r}_t = \tilde{\mathbf{y}} - T_t \theta_t$
 7. Break if $T_t = T_{t-1}$ or $\|\mathbf{r}_t\|_2^2 \leq \epsilon$
-

Output: sparse representation vector \mathbf{x}

The CcStOMP algorithm introduces a distance criterion into the algorithm and adjusts the classification accuracy by the maximum distance parameter mdis . The setting of the mdis param-

ter is briefly discussed here. When $mdis$ tends to 0, the clustering result includes only one atom per class, so the CcStOMP algorithm degenerates to the StOMP algorithm; When $mdis$ tends to ∞ , the atoms satisfying the queue criterion will belong to the same class, so the CcStOMP algorithm degenerates to the OMP algorithm. With the accuracy of atom selections being considered, the clustering shrinkage algorithm has clear and controllable upper and lower bounds. The introduction of the maximum distance parameter does not affect the convergence, thus the algorithm has good robustness.

3.2. Random Forest classification

In fault classification recognition, the classifiers' role is to determine the type of fault to which the test sample belongs based on well-labelled training data with different fault types. Linear regression and SVM are frequently employed as binary classifiers and are not suitable for classifying a wide range of faults. Neural network classifiers can affect the speed of fault identification due to their slow convergence rate. Therefore, random forest is chosen as the method for classifying and identifying motor ITSC faults.

The basic structure of a random forest is a decision tree, and the main mathematical description of a decision tree is as follows: let the sample set S have m categories C_i : ($i = 1, 2, \dots, m$), s_i is the number of samples belonging to C_i , then the sample expectation entropy is

$$I(s_1, s_2, \dots, s_m) = - \sum_{i=1}^m \frac{s_i}{s} \log_2 \frac{s_i}{s}, \quad (6)$$

where s and s_i denote the total number of samples and the number of samples belonging to category C_i respectively. For a single feature A of a sample, its expected entropy is

$$E(A) = \sum_{j=1}^k \frac{s_{1j} + s_{2j} + \dots + s_{mj}}{s} I(s_{1j}, s_{2j}, \dots, s_{mj}), \quad (7)$$

where k denotes the total number of sample features and s_{ij} denotes the i -th dimensional feature of the sample belonging to the category where

$$I(s_{1j}, s_{2j}, \dots, s_{mj}) = - \sum_{i=1}^m \frac{s_{ij}}{s_j} \log_2 \frac{s_{ij}}{s_j}. \quad (8)$$

The entropy gain of feature A can be obtained

$$\text{Gain}(A) = I(s_1, s_2, \dots, s_m) - E(A). \quad (9)$$

The entropy gain rate $\text{Gain}'(A)$ is calculated as

$$\text{Gain}'(A) = \frac{\text{Gain}(A)}{\text{split Info}(s)}, \quad (10)$$

where

$$\text{split Info}(s) = \sum_{i=1}^m \frac{s_i}{|s|} \times \log_2 \frac{s_i}{|s|}. \quad (11)$$

The random forest consists of several decision tree structures, and the main process of its classification is shown in Fig. 2.

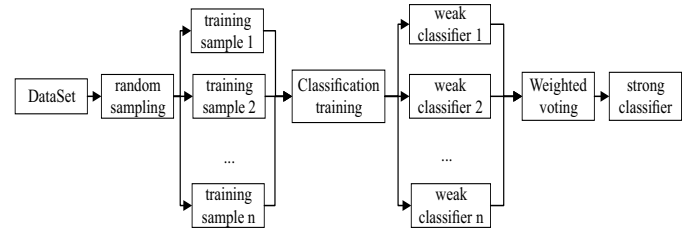


Fig. 2. Random forest process

Let a random forest consist of $h_1(X) h_2(X) \dots h_k(X)$ decision trees, for any two features X and Y of the sample, with edge functions

$$\begin{aligned} \text{ma}(X, Y) &= av_k(I(h_k(X) = Y)) \\ &\quad - \max_{j \neq Y} av_k(I(h_k(X) = j)), \end{aligned} \quad (12)$$

where $I(\cdot)$ denotes the transformation function, Y and j are the positive and negative categories determined by the random forest, respectively, $av_k(\cdot)$ denotes the mean value, and the value of $\text{ma}(XY)$ is proportional to the feature extraction effect.

RF have a significant advantage in handling high-dimensional data and demonstrates high adaptability to diverse data sets. Secondly, the advantage of RF is that the training speed is fast. The importance of variables is sorted according to certain rules. The implementation is relatively simple. The idea of the RF algorithm is that a new training set is generated by randomly selecting N sample subsets from the original sample training set with put-back repetitions, and then the RF consisting of N decision trees is generated. The new classification result is obtained by judging the selection result of each class by the decision tree. The subset of elements used to decide the ideal node splits approves weaker elements' representation in RF [24]. The Low correlation between trees in RF is executed by randomization of bootstrap sampling. RF perform well in applications for rotating machinery fault diagnosis.

4. EXPERIMENTAL RESULTS

4.1. Environment setup for measurements

In order to validate the proposed method in a real application, an experimental setup was constructed as shown in Fig. 3. In the experiments, the proposed algorithm was tested on an IPMSM with a pre-configured ITSC fault. The load was applied to the IPMSM via a coupling connected to the generator. In this experiment, we utilized the Siemens SIMATIC S7-1200 programmable controller, which supports PID control and closed-loop motion control functions. It provides three PID control loops with automatic adjustment functions for simple closed-loop process control. The implementation of experimental tests is composed of (1): External box enables importing the ITSC with different numbers of turns. (2): Current probes. (3): target IPMSM. (4): coupling. (5): Torque sensor. (6): Load motor.

Diagnosis of inter-turn short circuit fault in IPMSMs based on the combined use of greedy tracking and random forest

(7): Fixed base. (8): Encoder. (9) Touch Screen. (10): Digital signal processor(DSP). (11): PC. (12): Siemens SIMATIC S7-1200 programmable controller. (13): DC power supply.

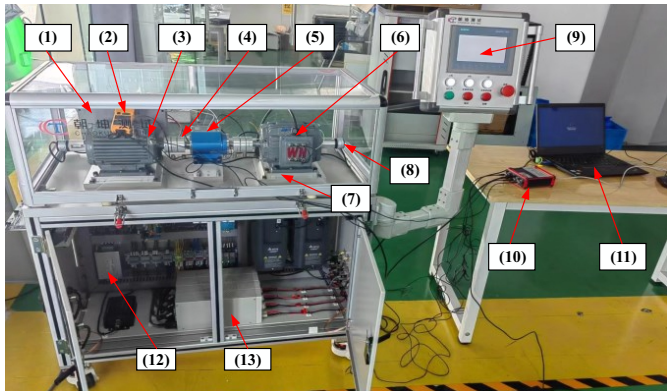


Fig. 3. Experimental setup

To simulate an internal short-circuit fault, the machine is rewound, and taps are made on 1–30% of the total number of coils in the A, B and C phase windings. The External box is connected and the terminals are led out. By connecting these taps it is possible to create ITSC faults with different numbers of turns on the motor. The percentage of short-circuit faults refers to the number of turns in the shorted abc phases divided by the total number of turns in each phase. The internal structure of a rewound motor and a detailed three-phase winding with taps is shown in Fig. 4.

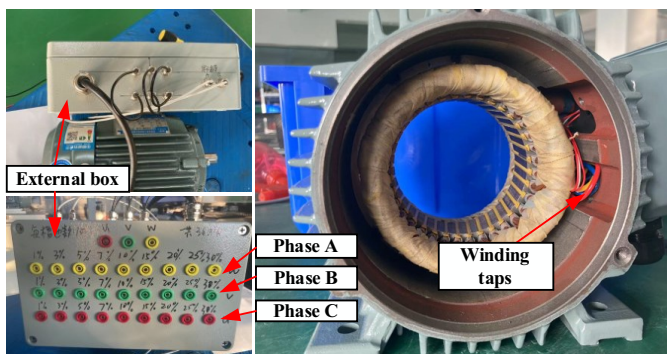


Fig. 4. Fault pre-processing

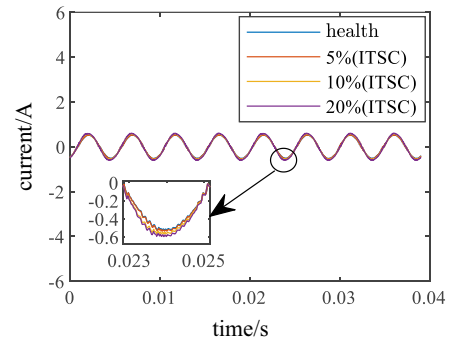
4.2. ITSC data acquisition

The IPMSM was driven by FOC at a rated speed (3000 r/min), and the data were collected for algorithm verification. All current and torque signals are sampled by the uTekL DSP at a sampling frequency of 51,200 Hz. When the motor is working at 3000 r/min, over 200 electrical cycles of data points are generated per second. The phase currents and torques of the IPMSM were measured at different loads under healthy, 5%, 10% and 20% short-circuit fault conditions during the test. The data obtained consists of a series of consecutive samples (480 samples), divided into two groups. Each sample contains 0.04 seconds of data.

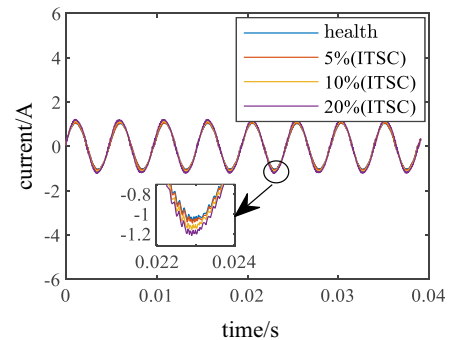
Group.1: 120 samples(3 × 40) for the healthy state of the motor under 3 loads (no-load, 1 Nm, 2 Nm).

Group.2: 360 samples(3 × 3 × 40) for the ITSC faults states of the (5%–10%–20%) shorted turns in phase A of the motor under 3 loads (no-load, 1 Nm, 2 Nm).

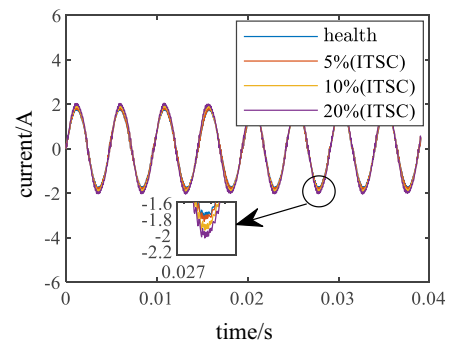
The current for the faulty phase and torque versus time curves (with a load of 2 Nm) are presented in Fig. 5 and Fig. 6, illustrating various failure rates.



(a) Phase A current at no load



(b) Phase A current at 1 Nm load



(c) Phase A current at 2 Nm load

Fig. 5. The change of phase current under different failure rates

As shown in Fig. 5 as the severity of the fault increases, the magnitude of the current increases accordingly. As the load increases, the magnitude of the increase in fault phase current also gradually increases. As shown in Fig. 6, the magnitude of the torque fluctuation increases correspondingly with the increase in fault severity. Combining the two characteristic signals, current and torque, can therefore improve the accuracy of the fault diagnosis model.

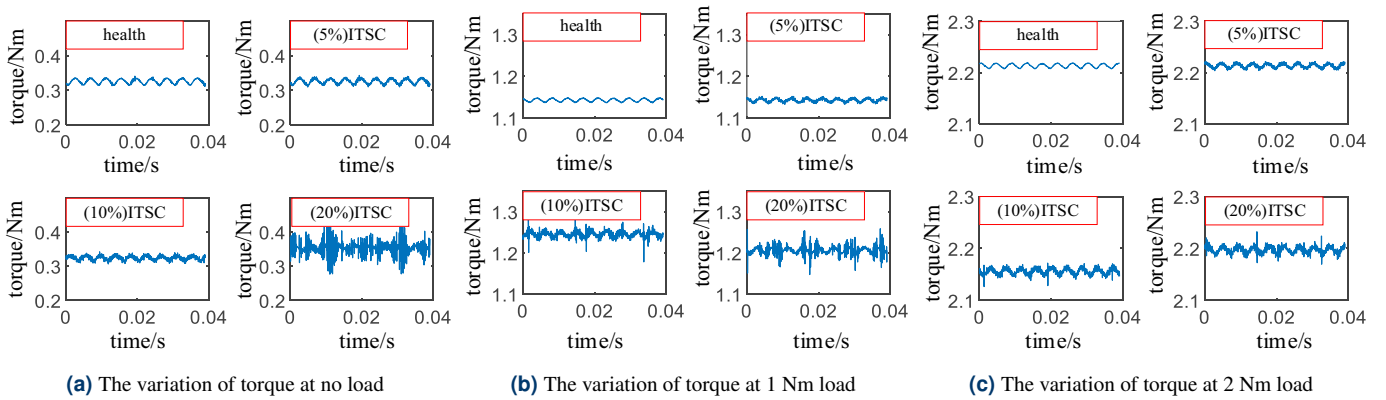


Fig. 6. The variation of torque under different failure rates

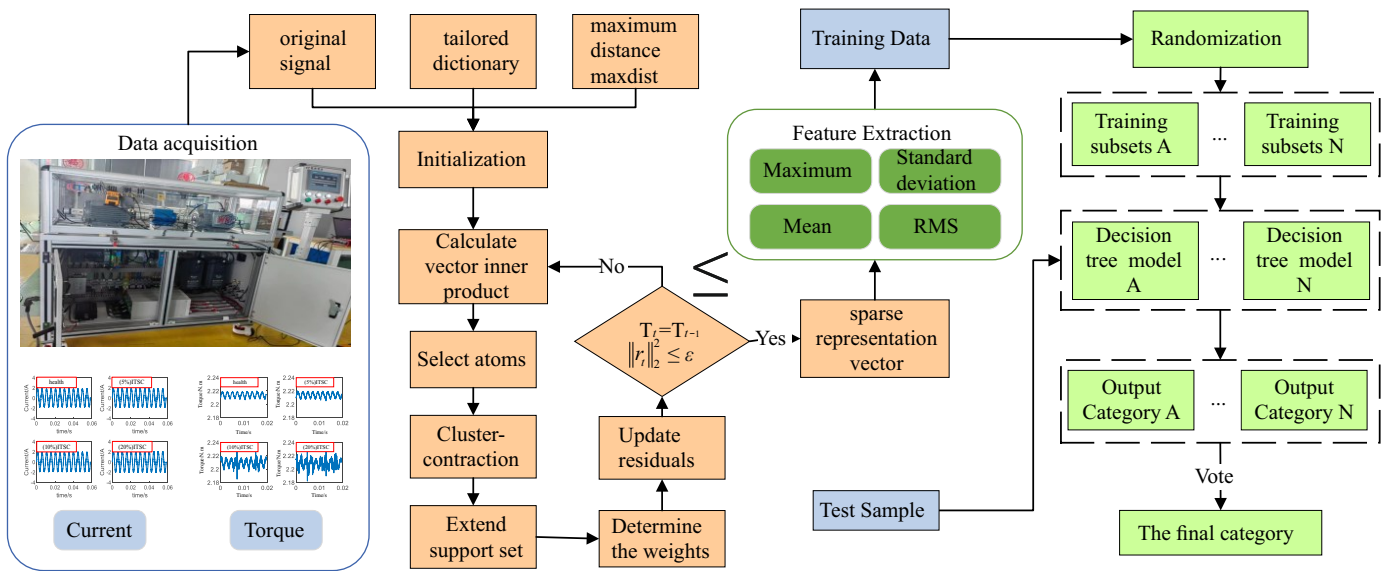


Fig. 7. General steps of the proposed diagnostic method

4.3. ITSC diagnosis

The general steps of the proposed diagnostic method are shown in Fig. 7.

4.3.1. Solve the sparse coefficients

Based on the constructed DTC-complete dictionary, the sparse coefficients are solved by the OMP, StOMP, and CcStOMP methods. The effectiveness of the sparse coefficient solution methods is quantified by evaluating the aforementioned methods based on both the speed of convergence and the sparsity of the resulting coefficients.

The average sparsity is defined:

$$MS = \frac{1}{m} \sum_{i=1}^m \frac{\|x_i\|}{\dim(x_i)}, \quad (13)$$

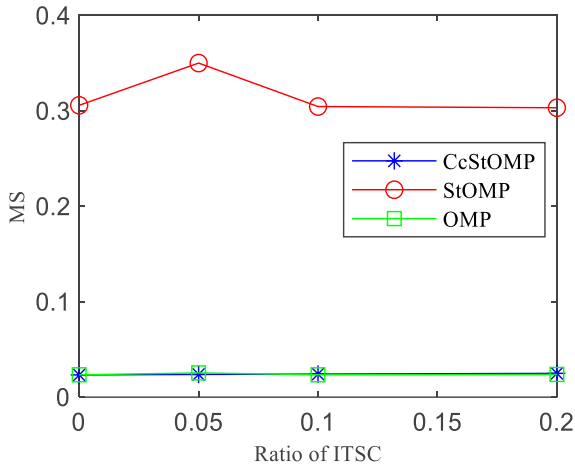
where x_i is the sparse vector and $\dim(\cdot)$ denotes the dimensionality of the vector.

The differences between the three sparse optimization algorithms in terms of the sparsity of the solution vectors are shown in Fig. 8a. The variation in the convergence of the residuals during the iteration process is illustrated in Fig. 8b.

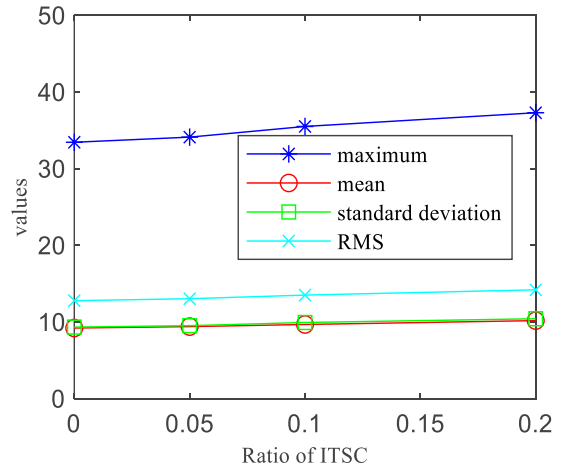
As can be seen in Fig. 8a, the sparse coefficients solved by applying OMP and CcStOMP maintain good sparsity, while the sparse coefficients of StOMP have a considerable number of redundant atoms, which leads to its higher average sparsity. From Fig. 8b, it can be found that CcStOMP and StOMP can achieve convergence quickly, while OMP requires more iterations to complete the matching. The CcStOMP algorithm can extract multiple target atoms at one time, which greatly improves the iterative efficiency. The average time of the three algorithms are shown in Table 1, which shows that the CcStOMP algorithm has higher computational efficiency.

Considering the average sparsity, convergence speed and time consumption, the CcStOMP algorithm was chosen as the final method for solving the sparse coefficients.

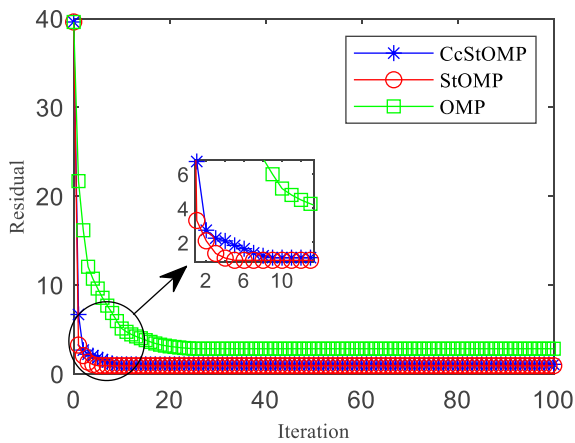
Diagnosis of inter-turn short circuit fault in IPMSMs based on the combined use of greedy tracking and random forest



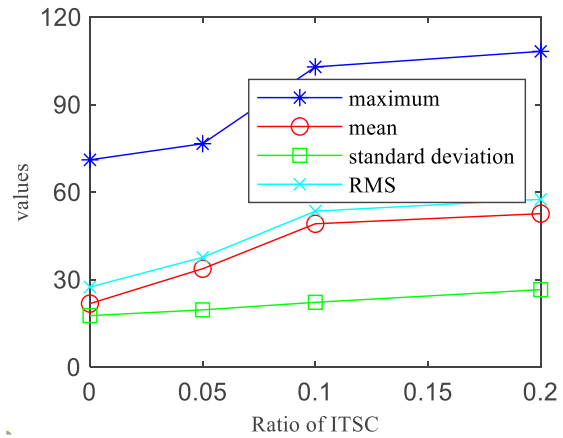
(a) Average sparsity of different ITSC fault ratios



(a) Sparse vector characteristics of current



(b) Residual convergence of the algorithms



(b) Sparse vector characteristics of torque

Fig. 8. The differences between the three sparse optimization algorithms

Fig. 9. Change of mean eigenvalue with different failure ratios

Table 1

The average time of the simulation

Description	CcStOMP	StOMP	OMP
Average time (s)	0.1542	0.1790	0.3149

4.3.2. Feature extraction

Multiple simulation experiments were carried out to solve the sparse coefficients for current and torque via the CcStOMP algorithm for different ITSC fault rates, respectively, selecting sparse coefficients of the current and torque signal sparse coefficient vectors. The maximum, mean, standard deviation and root mean square values were solved, and the average results from the multiple simulations are shown in Fig. 9. The eigenvalues of the sparse coefficients for the current increase slightly as the fault level increases. The eigenvalues of the sparse coefficients for torque are found to increase as the fault level increases.

Therefore, the sparse coefficient vectors of the current and torque signals are selected as the feature parameters, respectively. Their maximum, mean, standard deviation and root mean

square values are solved to form an 8-dimensional feature vector as the input random forest classification feature vector.

4.3.3. RF classification

The feature values were randomly divided into training and test sets. The training set data were imported to implement the construction of a RF classification model. The data was extracted from the test set for testing. Fault diagnosis results were compared with other machine learning algorithms. Machine learning methods include RF, Backpropagation Neural Network (BPNN), Convolutional Neural Network (CNN), Radial Basis Function Neural Network (RBFNN), and Support Vector Machine (SVM).

The curve of the error with the number of decision trees during the training process of the RF is shown in Fig. 10, which shows that the error decreases rapidly at the beginning as the amount of decision trees increases. When the number of decision trees is greater than 10, the error trend decreases gradually and slowly. A graph of the importance of each of the eight features is presented in Fig. 11. The three most informative features are the maximum and mean values of torque sparsity coefficients and the maximum value of the current sparsity coefficients.

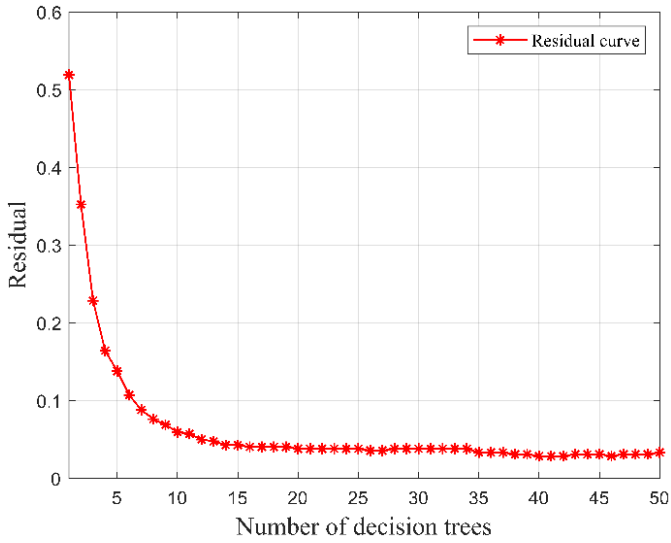


Fig. 10. The residual varies with the number of decision trees

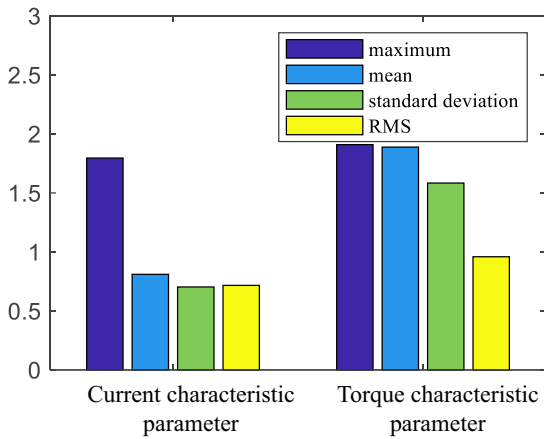
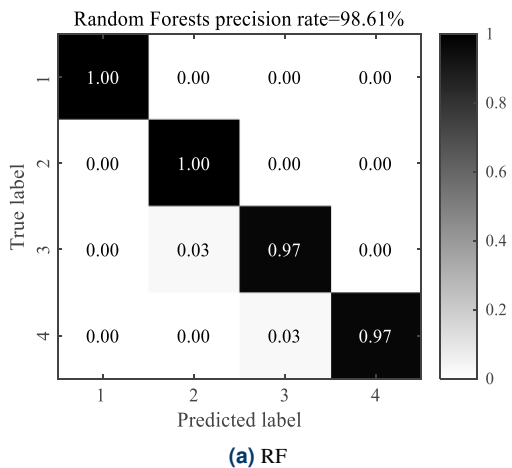
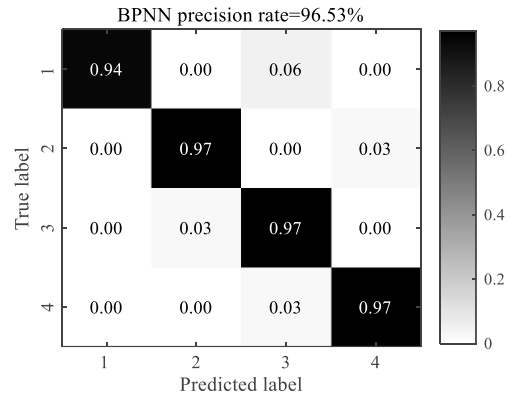


Fig. 11. The importance of each feature

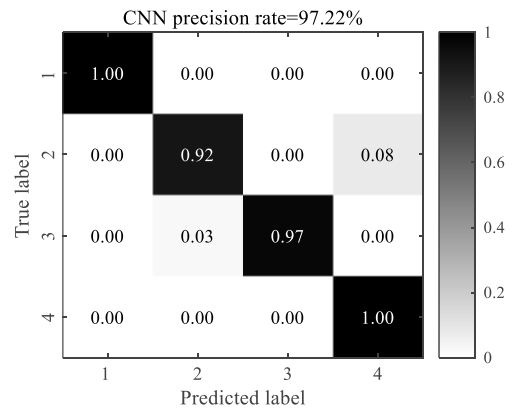
The confusion matrix of the prediction results of each algorithm is shown in Fig. 12. Label 1 represents the healthy state, and label 2 represents 5% inter-turn short circuit fault, and label 3 represents 10% inter-turn short circuit fault, and label 4



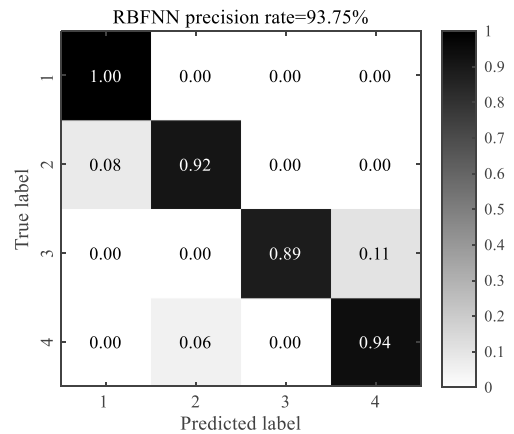
(a) RF



(b) BPNN



(c) CNN



(d) RBFNN

Fig. 12. The confusion matrix of the prediction results

represents 20% inter-turn short circuit fault. This figure clearly shows that the RF algorithm has a high advantage in prediction accuracy, with a prediction accuracy of 98.61%.

5. RESULTS AND DISCUSSION

The outcomes of training the feature vectors using different machine-learning algorithms are shown in Table 2. Above all, we used all 8 characteristics to train and test the RF with a pre-

Table 2
Comparison between RF and other machine learning algorithms

Classifier	All characteristics			The maximum and mean values of torque sparsity coefficients, the maximum value of the current sparsity coefficients		
	accuracies-mean	accuracies-STD	Time (s)	accuracies-mean	accuracies-STD	Time (s)
RF	98.61	0.01	2.532	97.91	0.01	1.056
BPNN	96.53	0.03	2.396	94.44	0.04	1.351
CNN	97.22	0.02	17.529	95.14	0.04	7.675
RBFNN	93.75	0.05	3.823	90.97	0.06	1.479
SVM	92.36	0.1	2.201	91.65	0.1	0.873

diction accuracy of 98.61%. Next, we diminished the number of characteristics by significance. The subsequent 3 characteristics were used to train and test different sets of RF with the prediction accuracy of 97.91%.

RF was compared with other machine learning algorithms to assess its effectiveness. The results are shown in Table 2. We tested all algorithms using all eight features. RF outperformed all other classifiers in terms of overall performance. Although the learning time of Random Forest was slightly longer than that of BPNN and SVM, it had the highest average accuracy and stability. Even when utilizing only three features (the maximum and mean values of torque sparsity coefficients, and the maximum value of the current sparsity coefficients), RF consistently outperformed all alternative classifiers. For the other machine learning methods, reducing the number of characteristics resulted in a greater drop in classification effectiveness.

6. CONCLUSIONS

In conclusion, we presented a method for detecting ITSC faults in IPMSMs using greedy tracking and RF. Transient current and torque signals were collected from an IPMSM under various load conditions at the rated rotating speed during data collection, each associated with different ratios of ITSC fault. The advantages of three different greedy tracking methods were compared. CcStOMP was used to solve sparse coefficients due to its good sparse representation efficiency and convergence speed. In the context of fault feature learning and classification, various machine models were compared, revealing that the RF diagnosis method exhibited superior diagnostic accuracy and robustness. RF spent only 2.532 s of learning time and achieved a diagnostic accuracy of 98.61%. The accuracy was still 97.91% using only the three most important features. The combination of CcStOMP and RF ensures faster fault diagnosis and more comprehensive and accurate extraction of fault features, with higher resolution characteristics and better immunity to interference than conventional methods. The method is non-intrusive and can be extended and applied in condition monitoring and diagnosis of industrial motors.

The variation in speed is challenging to quantify, and as speed changes, it affects the alteration of motor parameters. We plan to

investigate the effects of different speeds and speed variations on the diagnostic algorithm. Fluctuations in load torque or changes in motor parameters can induce variations in motor characteristics. Temperature changes or alterations in inductance can also cause resistance variations. The aforementioned factors can indeed exert certain influences on fault diagnosis. Additionally, exploring the novel aspect of changes in motor rotation direction will be a focus of our in-depth research in the future.

ACKNOWLEDGEMENTS

This work is supported by the National Key Research and Development Program of China (Grant No. 2020YFB1600604) and the Key Research and Development Program of Shaanxi Province (Grant No. 2021LLRH-04-03-02).

REFERENCES

- [1] N. Soundirarajan, K. Srinivasan, and A. Baggio, "Lyapunov stability based sliding mode observer for sensorless control of permanent magnet synchronous motor," *Bull. Pol. Acad. Sci. Tech. Sci.*, vol. 70, no. 2, p. e140353, Apr. 2022, doi: [10.24425/bpasts.2022.140353](https://doi.org/10.24425/bpasts.2022.140353).
- [2] H. Qiu, Y. Zhang, C. Yang, and R. Yi, "Influence of the number of turns on the performance of permanent magnet synchronous motor," *Bull. Pol. Acad. Sci. Tech. Sci.*, vol. 68, no. 3, pp. 429–436, Jun. 2020, doi: [10.24425/bpasts.2020.133375](https://doi.org/10.24425/bpasts.2020.133375).
- [3] P. Pietrzak and M. Wolkiewicz, "Stator winding fault detection of permanent magnet synchronous motors based on the bispectrum analysis," *Bull. Pol. Acad. Sci.-Tech. Sci.*, vol. 70, no. 2, p. e140556, Apr. 2022, doi: [10.24425/bpasts.2022.140556](https://doi.org/10.24425/bpasts.2022.140556).
- [4] D. Bochao, C. Shumei, H. Shouliang, W. Guoliang, and X. Bingliang, "A Simple Diagnosis of Winding Short-Circuited Fault of PMSM for Electric Vehicle," in 2012 *IEEE Vehicle Power and Propulsion Conference (VPPC)*, Korea (South), 2012, pp. 88–91, doi: [10.1109/VPPC.2012.6422577](https://doi.org/10.1109/VPPC.2012.6422577).
- [5] J. Hang, S. Ding, J. Zhang, M. Cheng, W. Chen, and Q. Wang, "Detection of Interturn Short-Circuit Fault for PMSM With Simple Fault Indicator," *IEEE Trans. Energy Convers.*, vol. 31, no. 4, pp. 1697–1699, Dec. 2016, doi: [10.1109/TEC.2016.2583780](https://doi.org/10.1109/TEC.2016.2583780).
- [6] Y.-L. He *et al.*, "Impact of Stator Interturn Short Circuit Position on End Winding Vibration in Synchronous Generators," *IEEE*

- Trans. Energy Convers.*, vol. 36, no. 2, pp. 713–724, Jun. 2021, doi: [10.1109/TEC.2020.3021901](https://doi.org/10.1109/TEC.2020.3021901).
- [7] J. Hang, J. Zhang, M. Xia, S. Ding, and W. Hua, “Interturn Fault Diagnosis for Model-Predictive-Controlled-PMSM Based on Cost Function and Wavelet Transform,” *IEEE Trans. Power Electron.*, vol. 35, no. 6, pp. 6405–6418, Jun. 2020, doi: [10.1109/TPEL.2019.2953269](https://doi.org/10.1109/TPEL.2019.2953269).
- [8] P.C.M. Lamim Filho, R. Pederiva, and J.N. Brito, “Detection of stator winding faults in induction machines using flux and vibration analysis,” *Mech. Syst. Signal Proc.*, vol. 42, no. 1–2, pp. 377–387, Jan. 2014, doi: [10.1016/j.ymsp.2013.08.033](https://doi.org/10.1016/j.ymsp.2013.08.033).
- [9] V. Hegde and M.G.S. Rao, “Detection of Stator Winding Inter-Turn Short Circuit Fault in Induction Motor Using Vibration Signals by MEMS Accelerometer,” *Electr. Power Compon. Syst.*, vol. 45, no. 13, pp. 1463–1473, 2017, doi: [10.1080/15325008.2017.1358777](https://doi.org/10.1080/15325008.2017.1358777).
- [10] S. Huang, A. Aggarwal, E.G. Strangas, B. Khoshoo, K. Li, and F. Niu, “Mitigation of Interturn Short-Circuits in IPMSM by Using MTPCC Control Adaptive to Fault Severity,” *IEEE Trans. Power Electron.*, vol. 37, no. 4, pp. 4685–4696, Apr. 2022, doi: [10.1109/TPEL.2021.3127538](https://doi.org/10.1109/TPEL.2021.3127538).
- [11] R. Cui, Y. Fan, and C. Li, “On-Line Inter-Turn Short-Circuit Fault Diagnosis and Torque Ripple Minimization Control Strategy Based on OW Five-Phase BFTHE-IPM,” *IEEE Trans. Energy Convers.*, vol. 33, no. 4, pp. 2200–2209, Dec. 2018, doi: [10.1109/TEC.2018.2851615](https://doi.org/10.1109/TEC.2018.2851615).
- [12] H. Liang, Y. Chen, S. Liang, and C. Wang, “Fault Detection of Stator Inter-Turn Short-Circuit in PMSM on Stator Current and Vibration Signal,” *Appl. Sci.-Basel*, vol. 8, no. 9, p. 1677, Sep. 2018, doi: [10.3390/app8091677](https://doi.org/10.3390/app8091677).
- [13] Y.-J. Goh and O. Kim, “Linear Method for Diagnosis of Inter-Turn Short Circuits in 3-Phase Induction Motors,” *Appl. Sci.-Basel*, vol. 9, no. 22, p. 4822, Nov. 2019, doi: [10.3390/app9224822](https://doi.org/10.3390/app9224822).
- [14] S. Shao, R. Yan, Y. Lu, P. Wang, and R.X. Gao, “DCNN-Based Multi-Signal Induction Motor Fault Diagnosis,” *IEEE Trans. Instrum. Meas.*, vol. 69, no. 6, pp. 2658–2669, Jun. 2020, doi: [10.1109/TIM.2019.2925247](https://doi.org/10.1109/TIM.2019.2925247).
- [15] T.A. Shifat and J.W. Hur, “An Effective Stator Fault Diagnosis Framework of BLDC Motor Based on Vibration and Current Signals,” *IEEE Access*, vol. 8, pp. 106968–106981, 2020, doi: [10.1109/ACCESS.2020.3000856](https://doi.org/10.1109/ACCESS.2020.3000856).
- [16] B. Yang, R. Liu, and X. Chen, “Fault Diagnosis for a Wind Turbine Generator Bearing via Sparse Representation and Shift-Invariant K-SVD,” *IEEE Trans. Ind. Inform.*, vol. 13, no. 3, pp. 1321–1331, Jun. 2017, doi: [10.1109/TII.2017.2662215](https://doi.org/10.1109/TII.2017.2662215).
- [17] Z. Zhang, Y. Xu, J. Yang, X. Li, and D. Zhang, “A Survey of Sparse Representation: Algorithms and Applications,” *IEEE Access*, vol. 3, pp. 490–530, 2015, doi: [10.1109/ACCESS.2015.2430359](https://doi.org/10.1109/ACCESS.2015.2430359).
- [18] H. Zhang, X. Chen, Z. Du, and R. Yan, “Kurtosis based weighted sparse model with convex optimization technique for bearing fault diagnosis,” *Mech. Syst. Signal Proc.*, vol. 80, pp. 349–376, Dec. 2016, doi: [10.1016/j.ymsp.2016.04.033](https://doi.org/10.1016/j.ymsp.2016.04.033).
- [19] W. He, Y. Ding, Y. Zi, and I.W. Selesnick, “Sparsity-based algorithm for detecting faults in rotating machines,” *Mech. Syst. Signal Proc.*, vol. 72–73, pp. 46–64, May 2016, doi: [10.1016/j.ymsp.2015.11.027](https://doi.org/10.1016/j.ymsp.2015.11.027).
- [20] D.L. Donoho, Y. Tsaig, I. Drori, and J.-L. Starck, “Sparse Solution of Underdetermined Systems of Linear Equations by Stage-wise Orthogonal Matching Pursuit,” *IEEE Trans. Inf. Theory*, vol. 58, no. 2, pp. 1094–1121, Feb. 2012, doi: [10.1109/TIT.2011.2173241](https://doi.org/10.1109/TIT.2011.2173241).
- [21] L. Song and R. Yan, “Bearing fault diagnosis based on Cluster-contraction Stage-wise Orthogonal-Matching-Pursuit,” *Measurement*, vol. 140, pp. 240–253, Jul. 2019, doi: [10.1016/j.measurement.2019.03.061](https://doi.org/10.1016/j.measurement.2019.03.061).
- [22] J. Fang, Y. Sun, Y. Wang, B. Wei, and J. Hang, “Improved ZSVC-based fault detection technique for incipient stage inter-turn fault in PMSM,” *IET Electr. Power Appl.*, vol. 13, no. 12, pp. 2015–2026, Dec. 2019, doi: [10.1049/iet-epa.2019.0016](https://doi.org/10.1049/iet-epa.2019.0016).
- [23] S. Liang, Y. Chen, H. Liang, and X. Li, “Sparse Representation and SVM Diagnosis Method for Inter-Turn Short-Circuit Fault in PMSM,” *Appl. Sci.-Basel*, vol. 9, no. 2, p. 224, Jan. 2019, doi: [10.3390/app9020224](https://doi.org/10.3390/app9020224).
- [24] J.C. Quiroz, N. Mariun, M.R. Mehrjou, M. Izadi, N. Mison, and M.A.M. Radzi, “Fault detection of broken rotor bar in LS-PMSM using random forests,” *Measurement*, vol. 116, pp. 273–280, Feb. 2018, doi: [10.1016/j.measurement.2017.11.004](https://doi.org/10.1016/j.measurement.2017.11.004).